



Smoothing of the down-skin regions of copper components produced via Laser Powder Bed Fusion technology

Valentina Candela^{1,2} · Matteo Pozzi³ · Eduard Chyhyrynets^{4,5} · Vanessa Garcia Diaz⁴ · Silvia Candela¹ · Razvan Dima¹ · Giacomo Favero^{1,6} · Cristian Pira⁴ · Adriano Pepato¹ · Piergiorgio Sonato^{7,8}

Received: 20 July 2022 / Accepted: 30 October 2022 / Published online: 10 November 2022
© The Author(s) 2022

Abstract

Additive manufacturing (AM) is revolutionizing the industrial scenario. Four copper samples have been printed via Laser Powder Bed Fusion (LPBF) at DIAM Laboratory (INFN—Sezione di Padova, Padova, Italy). Samples had different geometrical characteristics, to test the feasibility of the AM as a productive technique for the creation of unsupported copper structures that are characterized by surfaces with a very small inclination angle, where supports cannot be placed. Parts have been printed successfully even in case of 18° of inclination of unsupported walls with respect to the horizontal plane, and on the same samples, surface finishing treatments (performed by Rösler Italiana S.r.l. and INFN-LNL) have been performed to reduce the roughness of the down-facing surfaces. Indeed, the down-skin regions are the most critical areas of AM parts. Several surface treatments are under investigation: mass-finishing treatments (mechanical and chemically assisted mechanical processes), chemical polishing, and electropolishing, and for some of them, the results are extremely positive: from an initial roughness (Ra) of 30–35 μm , the treatments allowed us to achieve a Ra value lower than 1 μm . The study here exposed presents a good way to rapidly reduce the roughness of 3D-printed parts, reaching a mirror-like aspect.

Keywords Additive manufacturing · LPBF · Copper · Roughness · Surface finishing · Polishing

1 Introduction

AM technology is an innovative manufacturing technique, and, in some fields, it represents a revolutionary process, even though it was developed in the late 1980s [1]. Indeed, with AM it is possible to create geometrically complex components that could not be produced with subtractive and conventional manufacturing processes, such as turning or milling. Moreover, the AM allows to produce components very rapidly compared to the traditional processes, and at the same time the material waste is minimal [2, 3]. The aerospace and automotive industries are taking great advantage from this production method [4, 5]. AM seems to be peculiarly suitable also for the biomedical sector: indeed, the freedom of customization and the ability to produce complex-shaped implants make the AM an extremely interesting technology for creating patient-specific implants that replace, for example, hard tissues like bones. The technology can mimic the lost bone tissue with high accuracy, from mechanical, biological, and geometrical points of view [6]. Scaffolds created with the most suitable materials are then the best compromise that

✉ Valentina Candela
valentina.candela@pd.infn.it

¹ National Institute for Nuclear Physics (INFN) – Padova Division, Via Marzolo 8, 35131 Padova, Italy

² Centro Ricerche Fusione (CRF), University of Padova, Corso Stati Uniti, 4, 35127 Padova, Italy

³ Rösler Italiana S.r.l., Via Elio Vittorini 10/12, MB 20863 Concorrezzo, Italy

⁴ National Institute for Nuclear Physics (INFN) - National Laboratories of Legnaro, Viale Dell'Università 2, 35020 Legnaro, PD, Italy

⁵ Department of Chemical Sciences, University of Padova, Via Marzolo 1, 35131 Padova, Italy

⁶ Department of Management and Engineering, University of Padova, Str.lla S. Nicola 3, 36100 Vicenza, Italy

⁷ Department of Industrial Engineering, University of Padova, Via Gradenigo 6a, 35131 Padova, Italy

⁸ Consorzio RFX (CNR, ENEA, INFN, Università di Padova, Acciaierie Venete SpA), Corso Stati Uniti, 4, 35127 Padova, Italy

allows rapid tissue regeneration and integration, minimizing stress shielding and improving the cell adhesion phenomena [6]. Nowadays, a great number of materials can be additively manufactured, such as polymers (especially thermoplastic ones), ceramics, composites, and metals. In this paper metal additive manufacturing (also known as MAM) is concerned. The feedstock material could generally be a powder, a wire, or a sheet [5, 7].

There are several MAM methods available, such as Laser Powder Bed Fusion (LPBF), also known as Selective Laser Melting (SLM), where a laser is the energy source that melts the metallic feedstock; Electron Beam Melting (EBM), in this case, the energy source is an electron beam [2]; Direct Metal Laser Sintering (DMLS); or Direct Metal Deposition (DMD).

In this work, the LPBF technique was employed. It reaches high dimensional accuracy and high relative densities [2, 6]. A laser beam melts selectively a thin layer of powder that is laid onto a powder bed [1, 2, 5, 6, 8]; this layer is characterized by a certain thickness. On this, the laser scans the cross section of the object to be printed; then, a coater blade spreads another layer of powder; and the process repeats. The working principle is simple: parts are created layer-by-layer lasering the cross section of the objects at each layer, the objects are modeled in CAD software, and then the geometries are sliced; that is, they are virtually divided into many two-dimensional cross sections, one for each layer. The layer thickness can vary, depending on the material and the printing technique [2, 5, 6, 9]. Usually, a low-layer thickness is essential to reach the maximum density of the printed components; thus, also the mechanical properties can reach higher values. In some cases they achieve almost the same values as the bulk material. But generally, a compromise between layer thickness and final characteristics of the 3D-printed parts that must be achieved is found, because the more the layer is thin, the more the printing time increases, and this would raise costs.

The material properties depend on several factors: the process parameters and the microstructure influence the final performances of the parts [2].

Generally, an inert gas atmosphere inside the printing chamber is recommended for minimizing the oxidation of the material [5].

As previously mentioned, AM technology offers great advantages, especially where topological optimization and rapid prototyping are requested [1, 3, 10]. But on the other side, the technology could result very limited because of the poor surface quality of the AM parts [6, 10]; moreover, anisotropy and heterogeneity in microstructure and mechanical properties are frequent [7]. The defects that can be found in AM surface parts are due to several causes, such as staircase effect, lack of fusion, balling, and surface orientation [1, 6–8, 10].

The resulting surface roughness is often inadequate, and surface post-treatments are commonly engaged to reduce the irregularities that come from the printing process: indeed, imperfections can reduce the fatigue life of the components, wear, and scratch resistance [10]. Also, dimensional accuracy and aesthetics are strongly affected by surface quality [10].

In terms of roughness, the surface quality of 3D-printed components depends on the AM technique (PBF processes, DMD, etc.), the printing parameters, the characteristics of the feedstock material (the powder particle size distribution and particle shape), and the geometry of the part to be printed, but it also depends on the orientation of the surface itself with respect to the platform [6, 10, 11]. Here are summarized some typical surface definitions and a graphical representation is reported in Fig. 1:

1. Top surface: the surface that faces up and it is parallel to the substrate.
2. Vertical surface: the surface perpendicular to the substrate.
3. Lower surface: this surface is typically the one directly in contact with the powder.
4. Down-skin (downward facing surface): is the surface with an inclination angle smaller than 90° , with respect to the substrate [11]. This surface is very critical and generally the roughness is high, especially in the case of unsupported zones: here the surface touches the powder underneath, and the heat of the laser beam cannot be efficiently dissipated; thus, the heated and unmolten

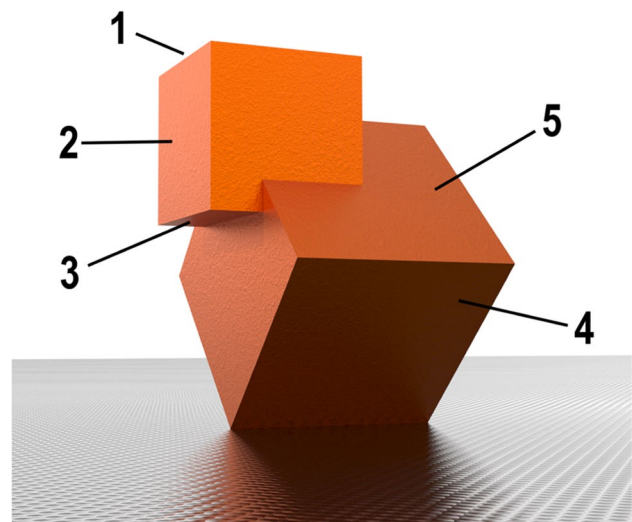


Fig. 1 In 3D-printed parts roughness strongly depends on surface orientation: **1** top surface, **2** vertical surface, **3** lower surface, **4** down-skin or downward facing surface, and **5** up-skin or upward facing surface

powder adheres to the surface increasing the final roughness [6].

5. Up-skin (upward facing surface): is the surface with an inclination angle bigger than 90° , with respect to the substrate [11]. This surface shows generally a good finish because the heat that comes from the laser can be rapidly dissipated by the underneath layers and the full beam exposure permits the complete melting of the powder [6].

For the down-skin and the up-skin, some printing parameters are more important than others: the contour parameters for instance are more influential than the core parameters for the final surface quality. Inclined surfaces are particularly challenging if the aim is to get very smooth surfaces; indeed, also the inclination angle and the stair-step effect are crucial: this latter comes from the intrinsic principle of the additive manufacturing technology since it is a layer-by-layer process [10, 11].

Generally, supports are recommended if the angle between the horizontal plane and the surface is smaller than 45° ; this would avoid distortions and part collapsing. A post-process is necessary to remove the support structures, and generally the surface finish is very poor. The minimum angle for unsupported surfaces strongly depends on the material.

Also, the inclination angle affects the quality of the surface. Commonly, the more the angle is small (with respect to the horizontal plane), the more the quality of the down-skin surface is poor [10].

The defects and the issues are generally the same for all the metallic materials processed via LPBF, but using copper powders, some aspects must be considered. Indeed, copper is one of the most reflective and highly conductive metals and, because of this, the LPBF process is critical [3, 12, 13]. Pure copper can exhibit a thermal conductivity of 400 W/mK in annealed conditions [3]; such high values cause rapid heat dissipation. Therefore the feedstock material does not melt completely, and the resulting scan-tracks are not regular and homogeneous. Moreover, copper reflects almost the total radiation if the laser wavelength drops into the infrared range (1000–1100 nm); consequently, the energy absorbed by the powder could be too low to create an appropriate melt-pool, especially if the maximum laser power is 400 W. Some studies have shown that less than 5% of the incident red laser energy is absorbed [3, 13]. Typically, copper alloys are more processable via LPBF with respect to pure copper, especially alloys containing elements that slightly decrease thermal and electrical conductivity [12].

Because of the aforementioned characteristics of the material, it is very hard to obtain copper AM parts with high relative densities; in other words, porosity is the main issue [3].

Surface roughness is typically very high on 3D-printed parts: rough surfaces are due to several aspects that have been already mentioned, such as the staircase effect, balling, and surface orientation, and also partially molten particles that remain stuck to the object increase the roughness [14]. The as-built faces can be smoothed by a wide range of treatments, and the entity of roughness reduction relies on the material and the method applied. For instance, milling is much more effective than blasting to reduce Ra in AM parts, Ti-6Al-4 V samples characterized by as-built surfaces with Ra of $17.9 \mu\text{m}$ reached a Ra value of $0.3 \mu\text{m}$ after machining and $10.1 \mu\text{m}$ after sand-blasting [15], but these two treatments are suitable in case the 3D-printed parts with simple and accessible geometry; electropolishing is another valid solution, thanks to its tunable smoothing action is suitable for AM parts of different materials: thanks to it, Jiang et al. obtained a surface Ra of $1.2 \mu\text{m}$ after 5-min-long treatment on Hastelloy X, starting from a roughness of $10.3 \mu\text{m}$ concerning planar surfaces, while for down-skin region, Ra decreased from 22.3 to $4.5 \mu\text{m}$ [14]. Surface post-treatments are then necessary to obtain a good and repeatable morphology of the surface because a good surface finishing improves both the esthetical and mechanical properties of the pieces [10]. Here is why this field is a growing area of interest.

Several techniques are available, which rely on different physical or chemical principles.

In general, surface finishing treatments can be distinguished in different ways:

- By the smoothing process: the surface can be smoothed removing the top layer of material, eliminating the outermost region that is characterized by the imperfections, or applying a plastic deformation that alters the initial surface, such as machining and sandblasting, respectively [10];
- By the nature of the smoothing agent: solid bodies, chemical solutions, electromagnetic waves (lasers), plasmas, or electric currents are just some of the available media;
- By the scale of their action: some treatments are suitable for reducing the macro-roughness, whereas others are appropriate for polishing; they act especially on the micro-roughness.

In some cases, the smoothing action of the media is supported and enhanced by vibrational or rotational movements of the objects to be treated (concerning mechanical treatments, such as Barrel Finishing or Vibro-Tumbling) or the stirring of the solution (in the case of chemical treatments) [16, 17]. Hybrid finishing treatments can also be adopted: in this case, media of different compositions are combined with the aim of accelerating the roughness

reduction or/and operating on macro- and micro-scale simultaneously.

In addition to the “traditional surface treatments,” coatings could provide a smoothening effect because the film fills the recesses and thus reduces the discrepancies between peaks and valleys of the surface.

In this work, conventional mass-finishing processes, chemically assisted mass-finishing processes, and chemical and electrochemical polishing have been applied to the additive-manufactured copper specimens. Operating conditions and principles are described in the next chapters and considerations on results will be exposed.

2 Materials and methods

The feedstock material for this work was a pure copper powder produced by Legor Group S.p.A. (Bressanvido, Vicenza, Italy). In Table 1, the chemical composition of the feedstock material is reported.

The metal powder is characterized by spherical particles since it has been produced by gas atomization. The morphology is visible in Fig. 2. This powder is very fine: its distribution is $D_{10}=12\ \mu\text{m}$, $D_{50}=19\ \mu\text{m}$, and $D_{90}=28\ \mu\text{m}$. Spherical particles are suitable for the LPBF technology because the resulting powder has a very high flowable rate and it can be properly spread onto the build platform to create a homogeneous layer.

The LPBF machine that has been used for printing the specimens is an EOSINT® M280 (Electro Optical Systems GmbH, Krailling, Germany); it is provided with a Yb red laser having a maximum power of 370 W; the wavelength of the laser is approximately between 1060 and 1100 nm. The laser spot diameter is 100 μm and it can scan a building area of $250\times 250\ \text{mm}^2$, while the maximum printable height is 325 mm. The printing chamber has been filled with a nitrogen atmosphere, and the oxygen level was kept below 0.5% during the printing process. The building platform can be heated up to 200 °C for decreasing the temperature gradients between the substrate and the part, thermal stresses are reduced, and a good bonding of the first layer is assured. The platform used in this work was made of stainless steel, which guarantees good adhesion of parts printed with copper, and the platform temperature has been set to 40 °C to avoid powder oxidation.

A prior parameter optimization campaign was done: the core of the different samples has been printed with the

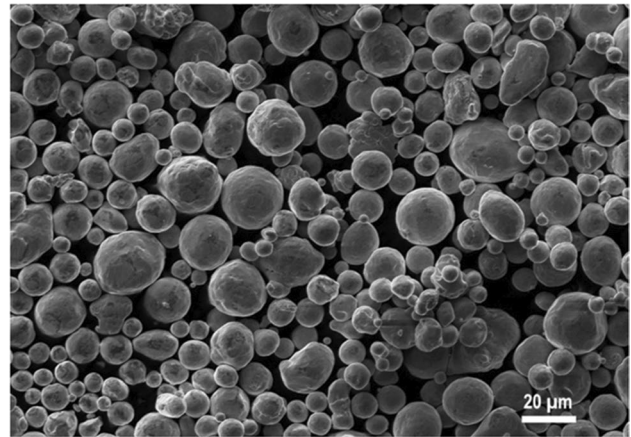


Fig. 2 SEM image of the pure copper powder used in this work

same combination of laser power (370 W), scanning speed (400 mm/s), hatch spacing (0.09 mm), and stripe width (5 mm) [18]; the down-skin parameters are different with respect to the core ones (laser power 150 W, scanning speed 1600 mm/s). The layer thickness was set to 20 μm .

Three different samples with three different sloping angles in the critical zone are investigated, keeping constant core and down-skin combination process parameters. The sloping angle variations of the samples (18°, 23°, and 28°) are shown in Fig. 3. The maximum external diameter of the samples is 49.5 mm.

The geometry of the samples wants to simulate half of the shape of an RF cavity; the dimensions refer to the 6-GHz superconductive cavity prototype. This geometry is particularly critical to print, and it is a good reference for this study.

The geometry in Fig. 3a represents half of ideal-cavity; the inclination angle was varied for some samples, since the limiting angle for pure Cu was unknown. The authors wanted to be sure that at least one of the three configurations was successfully printed.

2.1 Surface treatments

The surface treatments have been performed first by Rösler Italiana S.r.l. (Concorezzo, Monza Brianza, Italy), a company specialized in surface treatments, especially mass-finishing and shot blasting. Two different mass-finishing approaches have been evaluated and many steps have been carried out. Surface roughness of the parts was measured at the beginning (in as-built conditions) and after each step:

Table 1 Chemical composition (expressed in ppm, except for Cu element) of the feedstock pure copper powder

Cu	P	O	Sn	Zn	B	Fe	Mn	Pb
99.8 wt%	569	2495	500	700	6	10	1	55

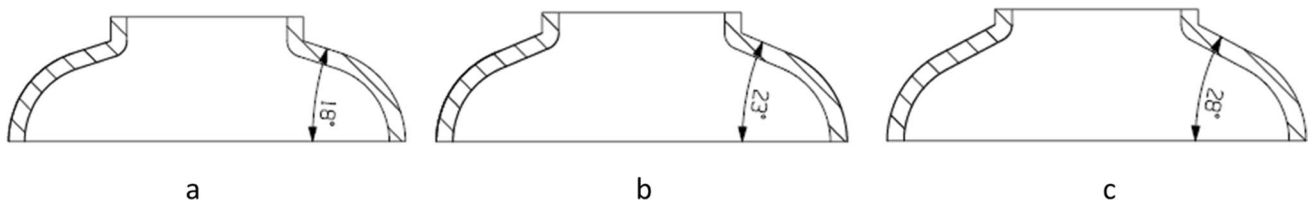


Fig. 3 **a** Original design with an inclination angle of the unsupported surface equal to 18° , **b** change of the geometry with a new inclination angle of 23° , and **c** 28° of inclination

the examined surface was the down-skin, since it is the most critical surface to be treated. In order to simulate the process realistically, two printed samples were coupled together during treatments, creating a cavity-like geometry (Fig. 4).

In this study, a pure mechanical mass-finishing treatment and a chemically assisted mechanical mass-finishing treatment were assessed: the two procedures have been applied on two different cavity-like assemblies. Here, different media, like abrasive ones, water and chemical compounds allow the surface smoothening thanks to the vibration and rotation of such reagents that flow inside the cavity-like assembly. The material removal is assured by the mechanical abrasion of the surface acted by the media.

2.1.1 Conventional mass-finishing treatment

This kind of process is a mechanical treatment that relies on the abrasion of the surface by means of solid media, which are metallic bodies with different sizes, and an abrasive paste. The smoothening action is obtained by the relative movement (vibration and rotation) of the sample to be treated with respect to the media: the test setup makes the abrasive agents flow inside and outside the cavity. With this treatment, roughness is reduced because the peaks on it are broken through a shear effect by means of the medium. Samples 1 and 2 have been treated this way; high-density media have been used in order to get a high abrasive action. Four different approaches were tested:

- 1) Use of spherical stainless-steel media, with different dimensions (to reach all the corners inside the sample, the spheres have a diameter that ranges from 3 to

- 5 mm) + abrasive paste (RSP 587, mainly composed of SiC, SiO₂ — cristobalite, and Al₂O₃).
- 2) Use of Cu needles (10 mm in length, with a diameter of approximately 2 mm) + abrasive paste (RSP 587).
- 3) Use of Cu needles + abrasive paste (corundum powder).
- 4) Use of Cu needles + abrasive paste (synthetic diamond powder).

All the media and the abrasive pastes are commercialized by Rösler Italiana S.r.l.

The first approach was maintained for 5 steps of the treatment; at step 6 the media was changed. Step 7 saw also a change in the abrasive paste; corundum powder has been used until step 8; then, from step 9 to step 10, the synthetic diamond powder has been employed.

Before the mechanical treatments, a sand-blasting pre-treatment (90 mesh corundum media at 3 bar for 3 min) has been carried out on sample 1, while sample 2, which showed a better surface finish, was directly treated without any preliminary operations.

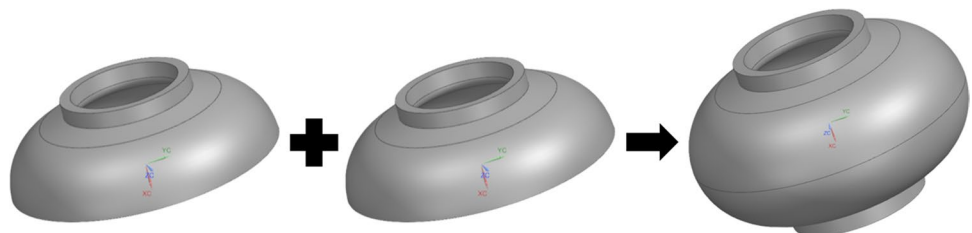
Each step of mechanical treatment lasted about 24 h, and the abrasive paste was renewed every 8 h. A total of 10 mechanical steps were conducted, and roughness has been recorded after each one; surface images have been also taken at the optical microscope.

2.1.2 Chemically assisted mass-finishing treatments

Chemically assisted tests were then assessed on the remaining sample 3 and sample 4 starting from the as-built conditions.

Ceramic spherical-shaped media (Rösler media RMBD1), with different dimensions (diameter 3–8 mm), were used

Fig. 4 Assembly of two halves to simulate the treatment of a complete cavity. The two halves have been kept in position with a sample holder during the treatment steps



for the treatment, together with the Rösler compound CMP 03/21 L (composed of inorganic acids and halogen compounds), specially developed for Cu alloys: ceramic material is chemically inert and does not react with the compound. It is a batch process; a single step lasted about 24 h, as the mechanical tests, but the chemical solution was renewed every 2 h. Five steps have been conducted; the concentration of the compound was increased progressively and so the smoothening effect.

Samples 1 and 2 were also subjected to the chemically assisted mass-finishing treatment after the mechanical one: in this case, the media used are a mixture of ceramic spheres and synthetic diamond powder, with the addition of the smoothening action of the chemical compound.

Once the resulting roughness of the samples was lower than 1 μm , the samples have been processed at Laboratori Nazionali di Legnaro (INFN, Legnaro, Italy). In particular, two approaches have been adopted and will be described in the next two paragraphs (Sections 2.1.3 and 2.1.4).

2.1.3 Chemical polishing solution (SUBU5)

SUBU is a chemical polishing solution developed at CERN. A SUBU bath chemical etching method was developed for LEP2 at CERN for processing 500-MHz and 350-MHz cavities. Two SUBU etchant solutions were developed, SUBU5 and SUBU20, which are composed of the same reagents, but in different concentrations. The name SUBU derives from its two main compounds: SU — sulfamic acid, and BU — butanol. For this work, SUBU5 was employed.

This treatment is usually done on traditionally produced copper cavities to clean and smooth the inner surface [19]. SUBU5 solution contains sulfamidic acid ($\text{H}_3\text{NO}_3\text{S}$ — 99.0%, 5 g/L), hydrogen peroxide (H_2O_2 ; 30%, 50 mL/L), n-butanol ($\text{C}_4\text{H}_{10}\text{O}$ — 99.9%, 50 mL/L), and ammonium citrate ($\text{C}_6\text{H}_{11}\text{NO}_7$ — 99.0%, 1 g/L) [19–22]. The treatment time can vary depending on the final requirements since the smoothening rate depends on the sample surface/solution volume ratio [20, 21]. Before the treatment, the substrate is cleaned in the ultrasound bath with GP17.40 commercial soap. After SUBU5 polishing, the sample is placed into a diluted solution of sulfamidic acid (~5 g/L) for passivation [19, 21, 22]. The polishing technique removes up to some microns of material; usually, the entity of the material removed depends on the method used for shaping the copper to create a cavity [19].

Samples 1 and 3 were subjected to this chemical polishing. The temperature during the treatment was set to $72\text{ }^\circ\text{C} \pm 2\text{ }^\circ\text{C}$. A magnetic stirring of the chemical solution was maintained during the etching. The total volume of the solution was 3.1 L. Samples have been soaked into the SUBU5 solution, moving them up and down.

2.1.4 Electropolishing (EP)

Electropolishing is gaining more and more interest as surface finishing post-treatment for 3D-printed parts; it is another well-known surface preparation process because it is suitable for geometrically complex and small objects [23], where other polishing technologies are not possible, as in the case of abrasive polishing. Moreover, this treatment can be applied to most of the metals and their alloys, also because the working principle is rather simple: the objects to be polished are immersed in a bath and they represent the anode of the electrical circuit. The bath is made of an electrolyte or a mixture of several compounds; the chemical nature of the electrolytic solution is specifically determined by the metal or the alloy that must be treated [20, 24]. Concerning copper, the electrolytic bath is made of phosphoric acid and butanol (volume ratio of 2:3). The process can be done at room temperature and the current intensity can vary: it can be higher in case a bath agitation is needed, or lower in case it is important to avoid bubbles formation [20].

A surface is characterized by a sequence of peaks and valleys: when a current and a certain voltage are applied, the surface is smoothed thanks to the dissolution of the peaks into the electrolytic bath. This happens because the electrical resistance of the peaks is lower than the resistance of the valleys; in other words, the current intensity is higher on peaks with respect to recesses: this leads to a selective action and thus a higher rate of dissolution of the tips [25].

Voltage, current density, and treatment time can be tuned to identify the optimal conditions for the specific application and material.

The technique is getting more and more interest also for additively manufactured components, where the geometrical constraints of the printed objects do not allow the exploitation of more traditional processes: fluid-based approaches like electropolishing (EP) can reach hidden areas very easily [23].

The advantage of EP is that it is a very quick process, compared to other processes such as Centrifugal Barrel Polishing (CBP) [26], but the minimum achievable R_a depends on the initial surface conditions because EP operates mainly on micro-roughness. So, EP is the final treatment in most cases.

Samples 2 and 4 were subjected to EP treatment. Voltage ranged between 5 and 2 V. The planar cathode was maintained at 1 cm from the samples.

In general, chemical polishing (SUBU) may produce pitting on the surface, while electropolishing (EP) allows to obtain a very smooth, morphologically homogeneous, and free of defect surface, like pitting or scratches, that indicates that it could be the most appropriate treatment for the preparation of the copper surface.

2.2 Roughness measurement

Roughness has been measured on the down-skin region (highlighted in Fig. 5) by means of the two-dimensional contact instrument Mahr Perthometer PGK120 (Mahr GmbH, Göttingen, Germany). Linear profiles have been evaluated (sampling length 5.6 mm, evaluation length 4 mm, cut-off 0.8 mm).

The recorded data need to be elaborated using filters because not all the irregularities are due to a rough surface; for instance, surfaces can be divided into periodic surfaces and non-periodic ones: for example, the former comes from traditional machining, such as turning, where the tool progressively creates grooves along the piece; in this case, a waviness filter must be applied. Otherwise, the shape of the surface alters the measurement. Non-periodic surfaces, on the other hand, are not characterized by a well-defined undulation. Most of the time the discrimination between periodic and non-periodic profiles is left to the discretion of the user, but it must be said that additive-manufactured surfaces can be treated as non-periodic, as in this work. In this specific case, a standard Gaussian filter has been applied and the measures have been performed on the most planar regions.

Roughness can be expressed by means of several parameters; the most important ones for the discussed case are exposed.

Ra: arithmetic average roughness or arithmetical mean height. It is a widely used parameter and it can be defined as the average value of the filtered roughness profile with respect to the center line within the evaluation length

(which is the length along a given direction used for assessing the profile under consideration).

$$Ra = \frac{1}{L} \int_0^L |Z(x)| dx \tag{1}$$

where *x* is the position at which the height of the profile *Z(x)* is evaluated. Clearly, a profilometer can measure discrete elements, so the integral becomes a summation:

$$Ra = \frac{1}{N} \sum_{i=1}^N |Z_i| \tag{2}$$

where *N* is the number of the acquired points and *Z_i* is the height of the generic acquisition point.

This parameter is useful for general quality control, but it does not describe the shape of the surface, because it takes into account only the height of peaks, not their width or frequency. Some surfaces can have the same *Ra* value, but their profile could be totally different.

Rp: maximum height of the peaks. This parameter indicates the distance between the mean line and the highest peak within the sampling length (which is the length along a given direction used for identifying the irregularities characterizing the profile under evaluation).

$$Rp = \max(Z(x)) \tag{3}$$

Rv: maximum depth of the valleys. It is similar to the *Rp* parameter, but it indicates the profile valley depth, that is, the lowest point of the deepest valley within the sampling length.

$$Rv = \min(Z(x)) \tag{4}$$

Rz: ten-point height. It indicates the sum of the average height of the five highest peaks and the average depth of the five deepest peaks within the sampling length. The exact definition of this parameter changes according to the considered standard (ISO, DIN, etc.).

$$Rz = Rp + Rv \tag{5}$$

Another parameter is *Rq*, which is the root-mean-square roughness of the assessed profile, evaluated within the sampling length. It represents the standard deviation of the distribution of surface heights.

$$Rq = \sqrt{\frac{1}{L} \int_0^L Z^2(x) dx} \tag{6}$$

The digital implementation becomes:

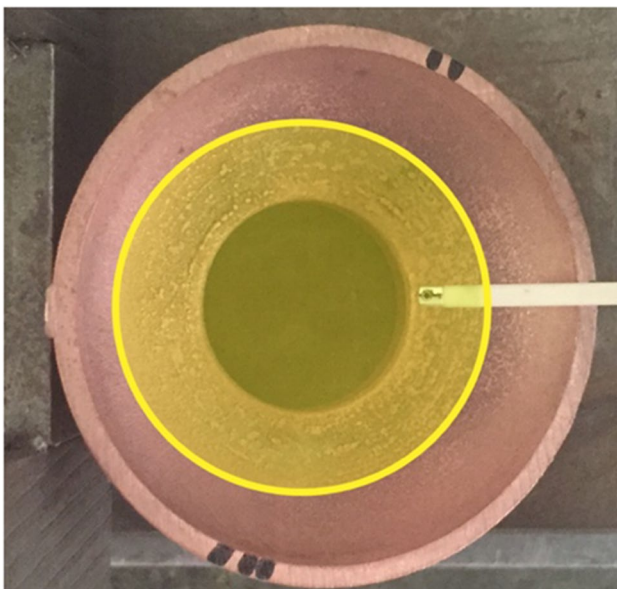


Fig. 5 The area highlighted in yellow is the examined region

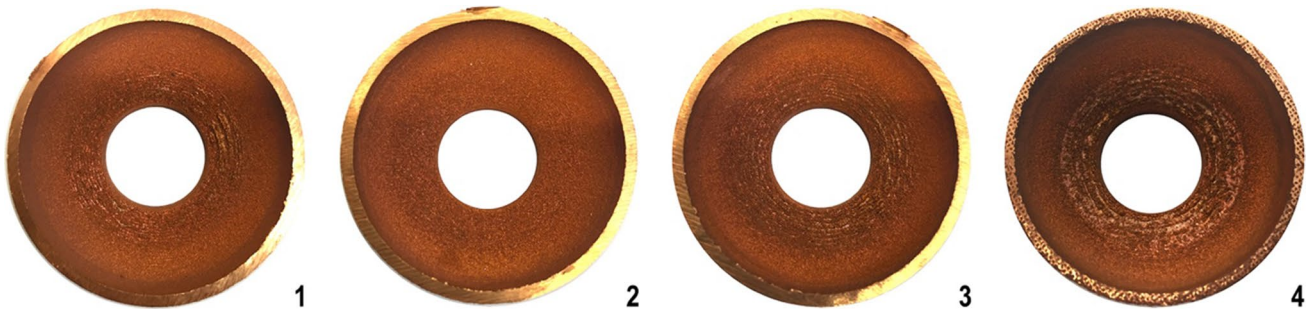


Fig. 6 Downward facing surfaces of the four samples. Sample 1 = 18°, sample 2 = 28°, sample 3 = 23°, and sample 4 = 18°

Fig. 7 Mass (a) and average roughness (*Ra*) (b) of samples 1 and 2

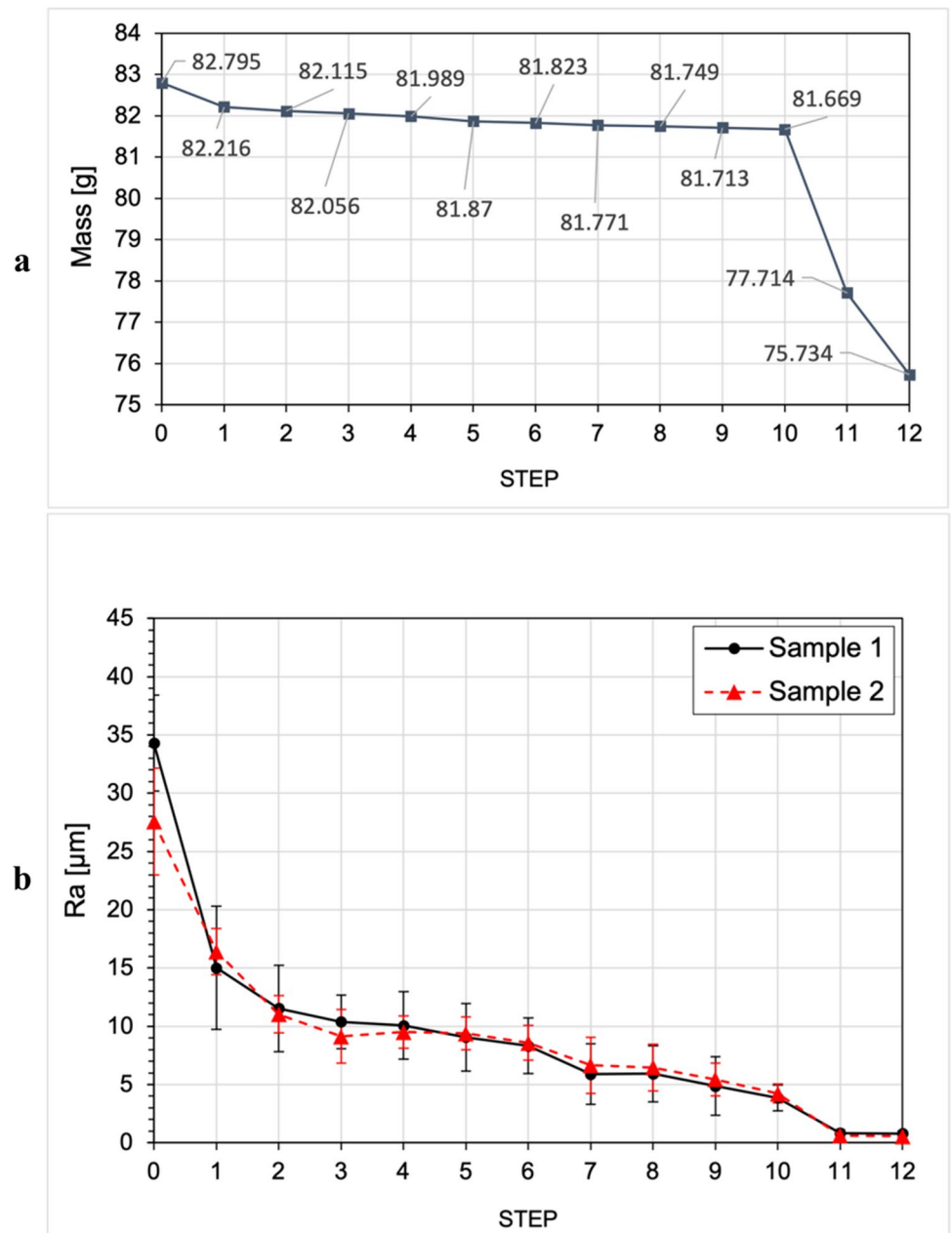


Table 2 Roughness measurement on samples 1 and 2 after each step

Sample no	Step no	<i>Ra</i> (μm)	<i>Rp</i> (μm)	<i>Rv</i> (μm)	<i>Rz</i> (μm)	<i>Rq</i> (μm)
1	As-built	34.3±4.1	73.4±9.4	93.5±1.0	167.0±20.5	42.6±5.8
	1	15.0±5.3	70.1±18.4	38.1±9.5	70.1±18.4	18.2±6.4
	2	11.5±3.7	21.0±6.9	33.1±10.9	54.1±17.5	14.4±5.0
	3	10.4±2.3	53.5±11.6	36.0±8.9	53.5±11.6	14.0±2.9
	4	10.1±2.9	17.7±5.2	28.6±5.5	46.3±10.5	12.7±3.3
	5	9.1±2.9	16.2±4.2	27.9±11.8	44.1±15.7	11.9±3.9
	6	8.3±2.4	16.1±4.6	30.5±2.9	46.6±10.7	12.0±2.9
	7	5.9±2.6	11.2±5.1	20.1±6.2	31.3±10.6	8.2±3.5
	8	5.9±2.4	11.0±4.2	19.6±9.3	30.6±13.3	8.5±3.4
	9	4.9±2.5	7.4±3.4	15.7±7.7	23.1±10.4	6.5±3.3
	10	3.9±1.1	7.8±2.5	13.6±2.6	21.5±5.0	5.0±1.1
2	1 ch-mec	0.8±0.3	1.4±0.4	2.7±0.4	4.2±0.7	1.2±0.5
	2 ch-mec	0.8±0.2	1.6±0.2	3.1±0.8	4.6±0.7	1.0±0.3
	As-built	27.6±4.6	63.4±13.5	63.9±6.2	127.2±19.2	33.7±5.6
	1	16.4±2.0	39.0±2.9	43.9±5.3	83.0±8.1	20.4±2.4
	2	11.0±1.6	19.3±3.1	31.3±2.8	50.6±4.8	13.4±1.4
	3	9.1±2.3	17.2±5.2	27.7±6.3	44.2±11.3	11.5±3.1
	4	9.5±1.4	17.4±2.8	34.9±5.6	52.3±6.2	11.8±1.9
	5	9.4±1.4	16.5±2.2	30.6±3.3	47.2±4.9	11.8±1.4
	6	8.6±1.5	15.0±2.7	30.4±4.2	45.4±6.6	11.2±1.6
	7	6.6±2.4	11.5±4.8	24.8±5.5	36.4±9.9	8.8±2.9
	8	6.5±2.0	11.9±2.9	23.7±3.9	35.5±6.7	8.7±2.0
9	5.4±1.4	8.9±2.4	17.7±3.8	26.6±5.3	6.9±1.4	
10	4.2±0.8	7.9±1.1	13.7±2.1	21.6±3.2	5.8±1.3	
1 ch-mec	0.6±0.2	1.1±0.3	2.2±0.3	3.8±0.3	0.80±0.3	
2 ch-mec	0.6±0.1	1.1±0.1	2.6±0.2	3.7±0.1	0.7±0.1	

$$Rq = \sqrt{\frac{1}{N} \sum_{i=1}^N Z_i^2} \tag{7}$$

Ra and *Rq* are similar, but *Rq* is more sensitive to the irregularities and changes of the profile than *Ra* and it is generally higher in value [27, 28].

Rp, *Rv*, and *Rz* are defined as discrete parameters because they refer only to a single peak, while *Ra* and *Rq* are not discrete because their values come from the assessment of an entire segment of a profile.

Five radial profiles have been assessed on each sample, and after each treatment step, the average results for each measure will be exposed in the next section.

2.3 Material loss

The material loss gives information on how much the treatment is aggressive: if the material removed is high, this could be an issue because it would mean that the geometry could sharply change; cavities are specifically designed to create a resonance with the working radiofrequency applied. Each specimen was weighed before and after each treatment

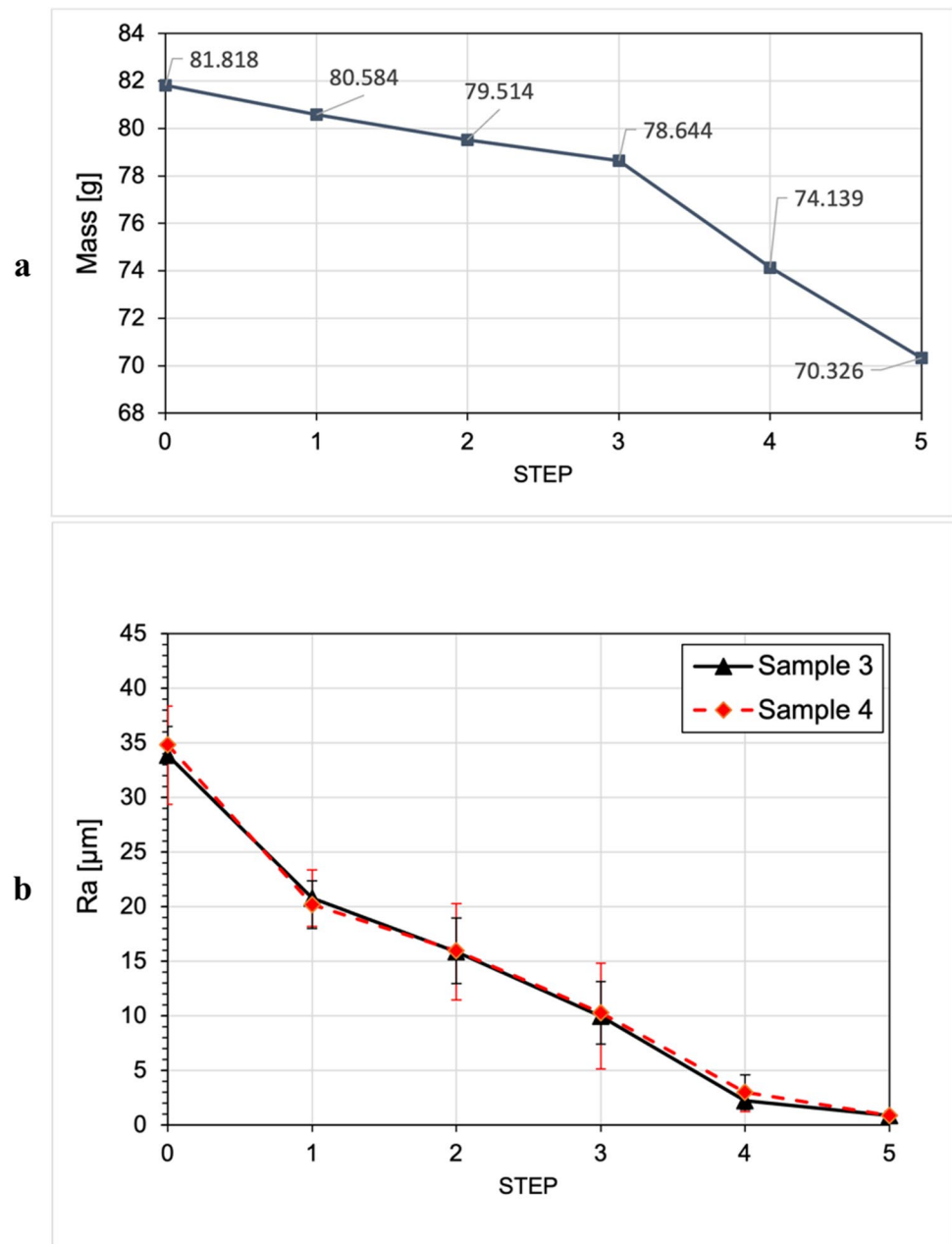
step, both for the mechanical and the chemically assisted treatments.

3 Results and discussion

The specimens have been printed successfully even with a minimum inclination angle of 18°. The quality of the down-skin was poorer for the sample with the minimum angle with respect to the samples with the angles of 23° and 28°. In Fig. 6 are reported the specimens upside-down to show the down-skin from the macroscopic point of view.

From Fig. 7, it is possible to see that mechanical treatments are good if it is necessary to quickly reduce the roughness, especially if the initial roughness is high, as in the case of the 3D-printed components. But after 4–5 steps the process does not improve the surface quality anymore: the *Ra* could not go below 9 μm. Other treatments were required, because *Ra* values were still too far from the target (1 μm), indeed some different media have been adopted: at step 6 Cu needles were used despite of spherical stainless-steel media of the previous steps; this is because copper density is higher than the stainless-steel’s one. Thus, the abrasive action is

Fig. 8 Mass (a) and average roughness (Ra) (b) of samples 3 and 4



higher; then at step 7 the abrasive paste was also changed, corundum powder replaced the RSP 587 abrasive paste, and from step 9 diamond powder replaced the corundum powder. The abrasive paste was changed due to the necessity of a higher abrasive action for removing a higher amount of material from the surface. The initial down-skin roughness ranged from 30 to 35 μm , in as-printed conditions. The mechanical treatment turned out to be very efficient during the initial stages since the roughness after the first step was a half with respect to the initial value (15–16 μm), and a third of the initial value after the second step (11 μm). Then the efficiency of the treatment decreased, and roughness followed an asymptotic behavior, here is why a change in the

abrasive paste and media was necessary. Indeed, different media allowed to enhance the smoothness of the surface, and at the end of step 10, a Ra of approximately 4 μm has been achieved. The material loss was also measured and after the first step the removed mass was less than 1 g; moving forward with the steps, the loss became lower and lower. Thus, the amount of the material removed resulted almost negligible. The trends of mass and roughness are visible in Fig. 7a and b, respectively, and roughness values are reported in detail in Table 2.

The mechanical mass-finishing process is quite efficient, especially at the first stages, but very slow. Moreover, the smoothing occurs only because of the cutting of the peaks,

Table 3 Roughness measurement on samples 3 and 4 after each step

Sample no	Step no	Ra (μm)	Rp (μm)	Rv (μm)	Rz (μm)	Rq (μm)
3	As-built	33.8 ± 4.5	74.3 ± 9.3	84.0 ± 7.0	158.4 ± 16.1	44.5 ± 2.2
	1	20.8 ± 2.6	37.1 ± 7.8	54.1 ± 3.9	91.2 ± 11.2	25.8 ± 4.4
	2	15.9 ± 4.4	26.2 ± 6.6	43.8 ± 2.9	69.9 ± 8.8	20.4 ± 4.1
	3	10 ± 4.8	17.3 ± 8.1	25.14 ± 9.0	42.4 ± 16.6	12.5 ± 5.5
	4	2.2 ± 1.0	3.7 ± 1.4	5.4 ± 1.1	9.1 ± 2.5	4.0 ± 2.9
	5	0.8 ± 0.4	1.7 ± 0.6	2.8 ± 1.0	4.5 ± 1.5	1.1 ± 0.6
4	As-built	34.8 ± 1.7	70.6 ± 2.2	85.0 ± 13.2	162.5 ± 13.3	38.9 ± 8.3
	1	20.2 ± 2.2	91.7 ± 11.6	52.6 ± 10.5	91.7 ± 11.6	25.8 ± 4.1
	2	15.9 ± 3.0	30.4 ± 6.3	33.6 ± 6.4	63.9 ± 13.5	18.8 ± 4.0
	3	10.3 ± 2.9	17.55 ± 4.0	26.9 ± 7.6	44.5 ± 11.5	13.7 ± 3.6
	4	3.0 ± 1.6	4.6 ± 2.3	7.5 ± 2.3	12.1 ± 4.6	4.2 ± 2.3
	5	0.9 ± 0.3	1.1 ± 0.3	2.9 ± 0.5	4.1 ± 0.7	1.1 ± 0.4

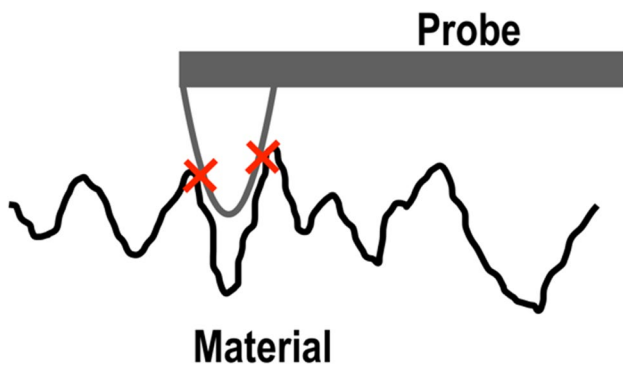


Fig. 9 If the tip radius is too big, the probe cannot analyze the deepest valleys, altering the roughness results

but the valleys remain, so a very long treatment would be necessary in order to eliminate the holes. Once the peaks are smoothed, roughness is mainly determined by the valleys; indeed, the decrease of Rp values is faster than the Rv ones

(Table 2). This means that an important amount of material should be removed to eliminate the negative discontinuities, and this causes a slowdown of the treatment effectiveness.

In addition, this treatment is suitable only for samples with a certain geometry: if the object has very small details or an intricate structure, the application of such treatment may not be recommended and efficient, because the medium could not reach all the corners and surfaces.

On the other hand, the chemically assisted treatment partly overcomes the issues of the mechanical treatment, because the chemical compound is aggressive and able to remove material from the surface itself: for this reason, the material loss (visible in Fig. 8a) is high and this is negative for the geometrical characteristics, as previously explained; however, it has a positive effect on the surface smoothening. Concerning samples 3 and 4, roughness decreased less rapidly with respect to the mechanical tests after the first three steps (the initial value was $\sim 34 \mu\text{m}$, as can be seen in Fig. 8b), so, starting from step 4, the chemical compound

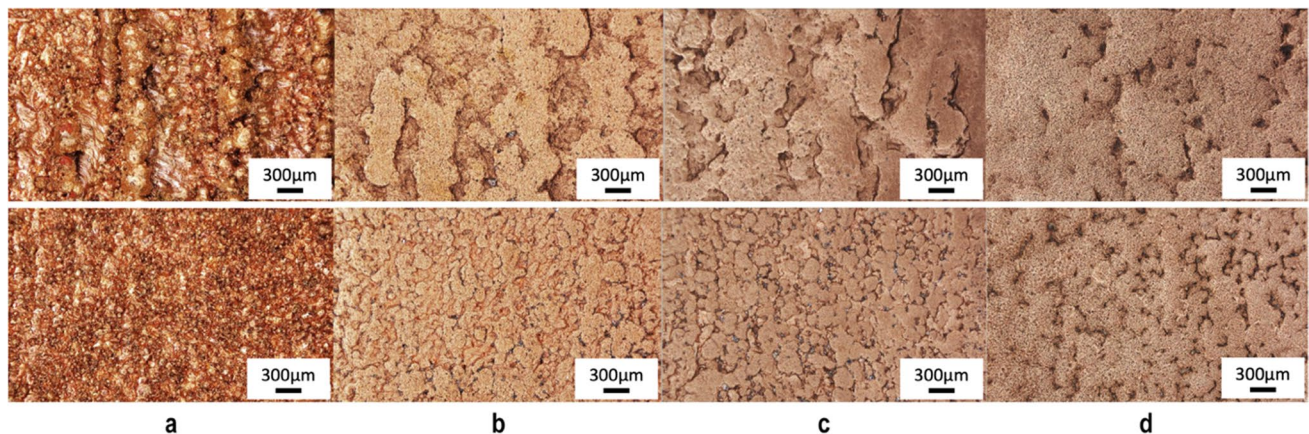


Fig. 10 OM images of down-skin surfaces of samples 1 (top) and 2 (bottom) in as-built conditions (a), after step 5 (b), after step 8 (c), and after step 10 (d)

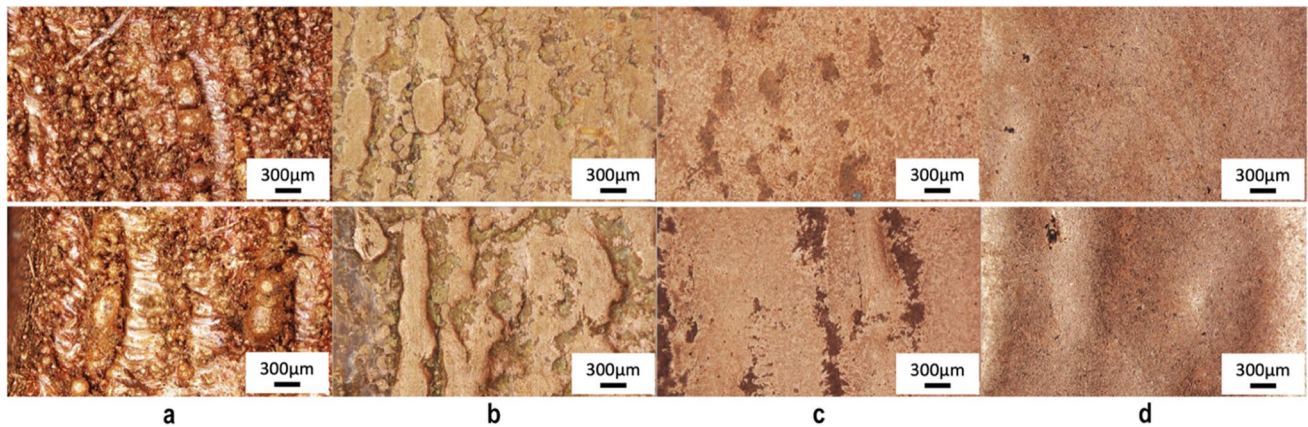
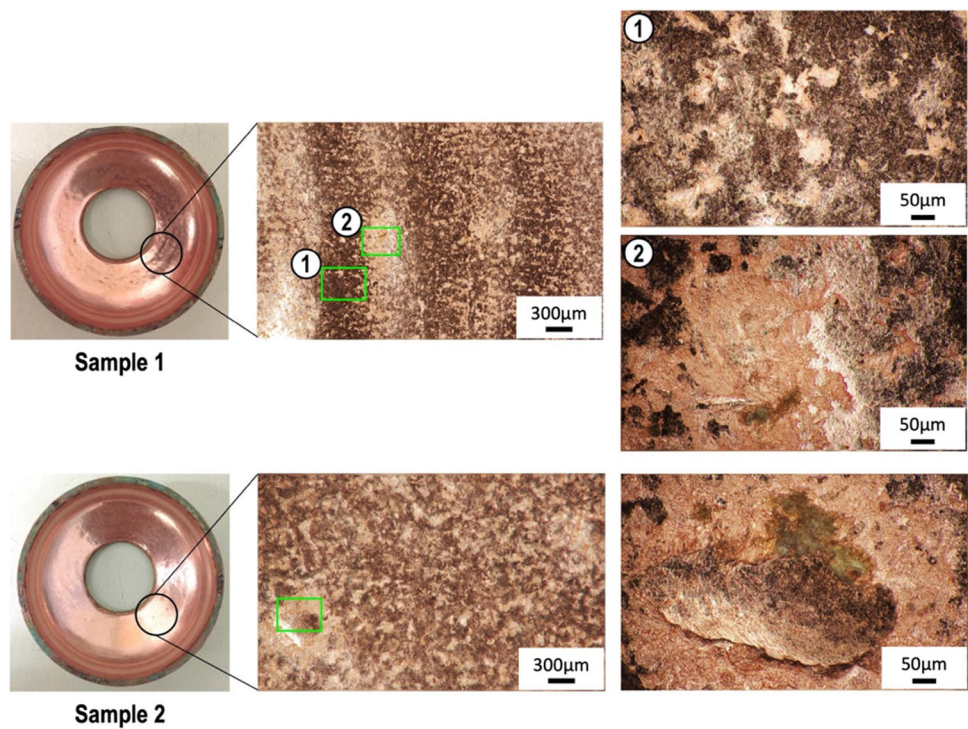


Fig. 11 OM images of down-skin surfaces of samples 3 (top) and 4 (bottom) in as-built conditions (a), after step 3 (b), after step 4 (c), and after step 5 (d)

Fig. 12 Details of sample 1 (top) and sample 2 (bottom) after two chemically assisted treatment steps: the surfaces show a different aspect with respect to samples 3 and 4. The action of the chemically assisted treatment was different



was used at a higher concentration. The roughness value decreased incredibly quickly after steps 4 and 5, and the R_a achieved roughly $0.8 \mu\text{m}$ (Table 3).

The chemically assisted treatment seemed to be the best choice between the two mass-finishing approaches for its capability in reducing roughness down to the target value. Nevertheless, the material loss is something that needs to be taken into account; in fact, for this treatment at least 10 g of material was lost for each specimen, while the total material loss due to the mechanical treatment is about 2 or 3 g.

However, it must be pointed out that the initial roughness value is surely underestimated: it could be more precise

saying that the initial roughness was higher than $30\text{--}34 \mu\text{m}$. This is due to the fact that a contact instrument might affect the roughness estimation, because this profilometer measures the surface imperfections touching the material with a probe tip (the usual tip radius is $2 \mu\text{m}$): the radius of the tip can be bigger than the space between two adjacent peaks. For this reason, the probe cannot analyze the deepest valleys of a surface (Fig. 9). Another problem of the contact profilometer comes up with “soft” materials: if the specimen to be analyzed is characterized by a very low hardness, the probe tip could scratch the surface, altering the measurement.

Fig. 13 OM images of down-skin surfaces of sample 1 (top) and 2 (bottom) after the first (a) and second (b) chemically assisted treatment steps performed. The surfaces are not homogeneous as in the case of samples 3 and 4

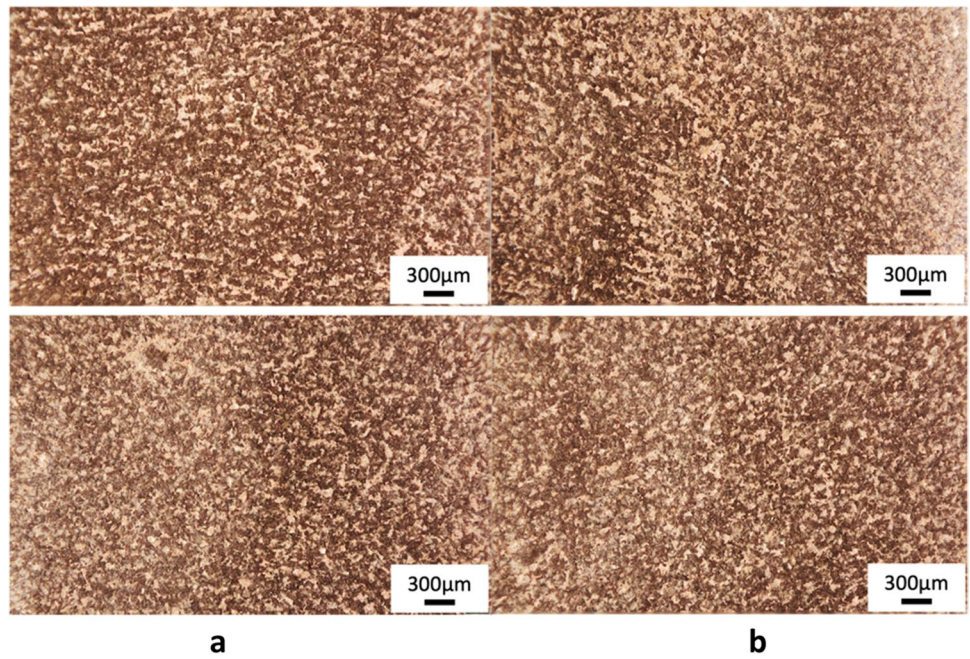
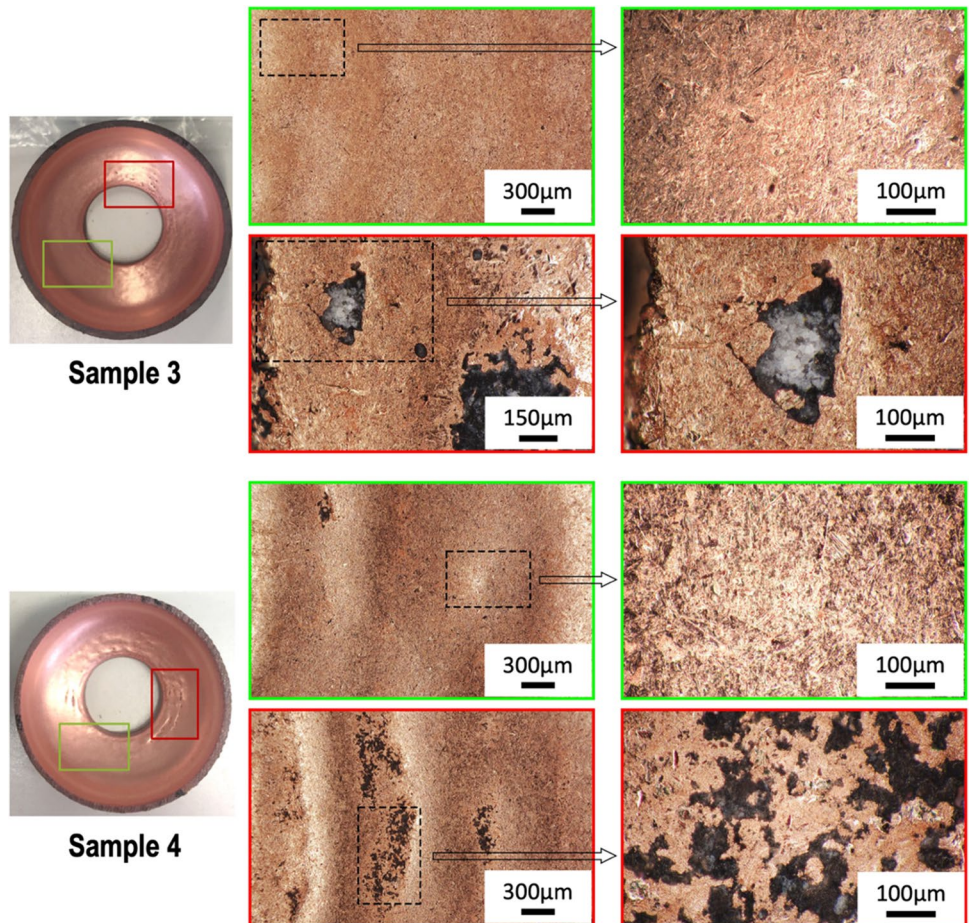


Fig. 14 Details of sample 3 (top) and sample 4 (bottom) captured with OM. Surfaces are generally very smooth, but some pores are extremely difficult to eliminate



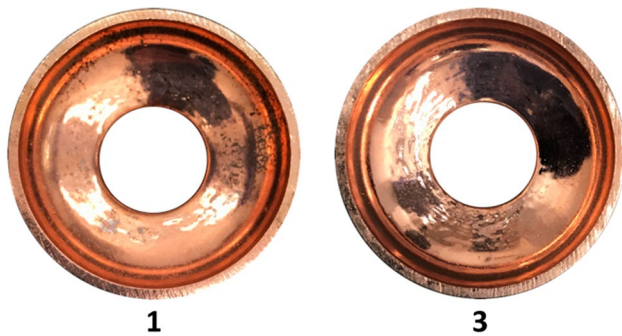


Fig. 15 Samples 1 and 3 after SUBU5. Dark spots, probably due to SUBU5 treatment, are clearly visible on the surface of sample 1

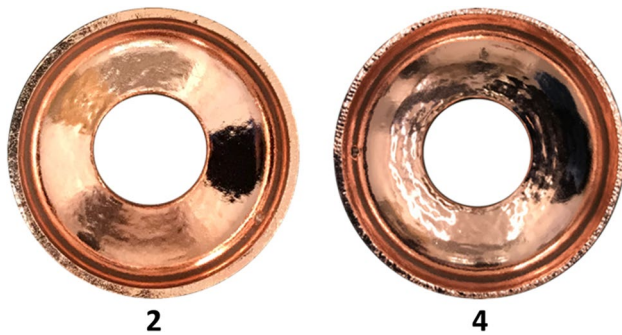


Fig. 16 Samples 2 and 4 after EP treatment

In both cases, the roughness measured is not the real one.

Concerning the surface aspect, it is evident how the conventional mass-finishing treatments work: on samples 1 and 2, peaks are smoothed and “cut” by the abrasive bodies while the valleys are not modified by the media (Fig. 10). On the other hand, chemically assisted mass-finishing processes performed on samples 3 and 4 are more homogeneous in their action: the whole surface (peaks and valleys) is etched by the chemical solution, and peaks are smoothed by the solid medium similarly to the mechanical treatments (Fig. 11).

However, it must be noticed that, after 10 steps of mechanical treatments, the chemically assisted treatments performed on samples 1 and 2 produced a completely different texture on the surfaces (Figs. 12 and 13).

At the same time, scratches and dark areas are clearly visible on the micrographs at higher magnitudes regarding samples 3 and 4 (Fig. 14): that could be caused by the manufacturing technology or by the solid (metallic or ceramic) media. Scratches are presumably due to the media, while the dark areas could correspond to artifacts generated by the additive manufacturing, maybe because of non-optimal printing parameters or because of the lack of supporting structure that contributed to generating irregular surfaces.

Despite the good Ra value achieved with chemically assisted treatments, bigger pores could not be eliminated easily, and they represent possible contaminated sites, because the reagent and waste compounds accumulate there, and they are extremely difficult to wash away (Fig. 14).

Samples 1 and 3 have been treated with SUBU5. The treatment lasted 13 min, and less than $10\ \mu\text{m}$ of material has been removed from the surface. The surfaces here are shiny and mirror-like (Fig. 15), but irregularities due to AM building process are evident: the surface is still wavy. In this case, it is possible to see some point-like defects on the internal surface (down-skin). The non-homogeneous behavior of the chemical polishing might be due to different grain orientation of the copper surface and/or the microscopic structures (pores or microscopic asperities) produced by AM. Literature [20, 22, 29] confirms the pitting produced by the treatment also on bulk copper samples; this could generate a higher surface roughness compared to the EP-treated surfaces. Samples 1 and 3 look similar, except for some dark areas on sample 1. These darker regions look like oxidized copper. Recent works [22] revealed that dark brown color develops on the surface of the substrate when acid is completely consumed and oxide formation starts; this happens when the final cleaning stage is not performed properly and a small amount of acid remains on the surface, but further investigations need to be carried out to understand if these spots and their distribution are caused by SUBU5, by the prior smoothening treatments (conventional mass-finishing treatment + chemically assisted mass-finishing treatment) or by the manufacturing method. The first two hypotheses seem to be the most realistic, considering that sample 3 does not show any spots.

Electropolishing was tested on samples 2 and 4; the treatment lasted 1 h and the process removed roughly less than $40\ \mu\text{m}$ of material. The action of the EP occurred

Table 4 Roughness measurements after the final surface treatments for all the samples

Sample no	Treatment	Ra (μm)	Rp (μm)	Rv (μm)	Rz (μm)	Rq (μm)
1	SUBU5	0.9 ± 0.2	1.6 ± 0.5	2.0 ± 0.6	3.7 ± 0.6	1.2 ± 0.3
2	EP	0.6 ± 0.1	1.1 ± 0.1	1.7 ± 0.2	2.8 ± 0.3	0.7 ± 0.1
3	SUBU5	0.4 ± 0.1	0.9 ± 0.2	1.3 ± 0.6	2.2 ± 0.8	0.6 ± 0.2
4	EP	1.1 ± 0.3	1.2 ± 0.4	2.9 ± 0.9	4.1 ± 1.3	1.3 ± 0.5

on the whole surface, not only the internal one; thus, the material removal concerns the entire surface.

The surface looks very smooth and bright, near to mirror-like aspect (Fig. 16), even though the irregularities due to the AM are still clearly visible, like on SUBU5-treated samples. There are no evident differences between samples 2 and 4 after the EP treatment, but the surface is wavier on sample 4 because of the 18° of inclination.

Roughness measurements after the polishing treatments revealed the smoothening action of EP and SUBU5 (Table 4). It is evident that Ra values are roughly the same with respect to the Ra reported in Tables 2 and 3, but generally, the values are higher, except for sample 3, which abundantly decreased the values. This could be due to the heterogeneity of AM surfaces; the measure could be strongly affected by the examined region. What is important to note is that the Rz roughness is lower than before polishing; this means that surfaces are more planar, and the difference between peaks and valleys is reduced. Surfaces are more uniform; indeed, the standard deviation is generally lower if compared to the values reported in Tables 2 and 3. As long as it is a discrete parameter, Rz could be a more reliable indicator with respect to Ra and Rq to evaluate the results, since Ra and Rq are averaged values and might not represent properly the surface conditions (i.e., different surfaces can show the same Ra values).

4 Conclusions

A preliminary analysis to demonstrate the quality assurance of surface finishing treatments was conducted on copper AM samples. Additive manufacturing of copper revealed to be a promising production technology also for peculiar geometries characterized by very low inclination angles of the downward facing surfaces. In the discussed work, the absence of supporting structures was mandatory, but the printing process showed that inclined copper structures with an angle of 18° can be printed without supports. Down-skin roughness of as-built samples is high for the design requests; thus, different finishing techniques have been investigated. To achieve the desired down-skin roughness, post-process treatments are essential: this is a general issue that can be referred to for the main metal powders processed via LPBF. In this work, conventional mass-finishing treatments quickly reduced the initial roughness and at the same time the material removal was minimal, but the effectiveness of such treatment decreased step after step. Chemically assisted mass-finishing processes, on the other hand, are easily tunable in their efficiency. Increasing the concentration of the chemical compound, the smoothening effect can go beyond the asymptotic behavior that characterizes the conventional process: the compound can penetrate into the valleys since

it has no hindrance, so the whole surface that is exposed is involved. However, even if the roughness reduction is more efficient, the material loss is extremely high if compared to the mechanical treatments, and this could be the main aspect that limits the application of such smoothening treatment. The post-processing could be optimized by combining the two procedures: initial mechanical treatment steps can drastically reduce the roughness, and then chemically assisted steps could be performed to achieve the targeted Ra value.

All the samples treated with mechanical or chemically assisted mass-finishing techniques achieved a down-skin roughness lower than 1 μm , starting from 30 to 40 μm in as-built conditions. To further increase the surface quality, further polishing treatments, such as EP (samples 2 and 4) and SUBU5 (samples 1 and 3), were implemented.

Both generated final mirror-like surfaces; the action was similar for samples characterized by a different smoothening history (i.e., SUBU5 was tested on sample 1 and sample 3, treated with conventional mass-finishing treatment + chemically assisted treatment and only chemically assisted treatment, respectively). But on the surfaces etched with SUBU5, pitting has been generated and sample 1 developed darker spots on its down-skin face, while the EP produced very smooth and homogeneous surfaces.

Further investigations and studies need to be carried out, in order to get the best as-built surface properties and reproducible results. Printing parameter optimization could lead to better down-skin homogeneity. Post-printing treatments need also to be optimized: it is necessary to create the best combination between mechanical treatments, chemically assisted processes, EP, and SUBU5 treatments, in order to get the most efficient procedure that minimizes the processing time (in terms of steps/treatment time for each process) and the material loss, and at the same time maximizes the smoothening action.

The finishing procedure, in this work, can be considered as a general purpose to treat irregular rough surfaces, typical of additive manufactured surfaces.

Author contribution The authors' contributions to the manuscript follow:

V. C.: conceptualization, investigation, methodology, validation, data curation, writing — original draft.

M. P.: conceptualization, investigation, methodology, validation, data curation, writing — review and editing.

E. C.: investigation, methodology, writing — review and editing.

V. G. D.: investigation, methodology.

S. C.: conceptualization, investigation, writing — review and editing.

R. D.: conceptualization, supervision.

G. F.: investigation, writing — review and editing.

C. P.: conceptualization, supervision.

A. P.: conceptualization, funding acquisition, supervision, writing — review and editing.

P. S.: supervision, writing — review and editing.

Funding Open access funding provided by Università degli Studi di Padova within the CRUI-CARE Agreement. This work was financially supported by I.Fast (Innovation Fostering in Accelerator Science and Technology) organization.

This work was developed with the financial support of Fondazione Cassa di Risparmio di Padova e Rovigo (CariPaRo).

This work has been carried out within the framework of the EUROfusion Consortium, funded by the European Union via the Euratom Research and Training Programme (Grant Agreement No. 101052200—EUROfusion). Views and opinions expressed are however those of the author(s) only and do not necessarily reflect those of the European Union or the European Commission. Neither the European Union nor the European Commission can be held responsible for them.

Data availability Not applicable.

Code availability Not applicable.

Declarations

Ethics approval Not applicable.

Consent to participate Not applicable.

Consent for publication Not applicable.

Competing interests The authors declare no competing interests.

Open Access This article is licensed under a Creative Commons Attribution 4.0 International License, which permits use, sharing, adaptation, distribution and reproduction in any medium or format, as long as you give appropriate credit to the original author(s) and the source, provide a link to the Creative Commons licence, and indicate if changes were made. The images or other third party material in this article are included in the article's Creative Commons licence, unless indicated otherwise in a credit line to the material. If material is not included in the article's Creative Commons licence and your intended use is not permitted by statutory regulation or exceeds the permitted use, you will need to obtain permission directly from the copyright holder. To view a copy of this licence, visit <http://creativecommons.org/licenses/by/4.0/>.

References

- Kruth JP, Froyen L, Van Vaerenbergh J, Mercelis P, Rombouts M, Lauwers B (2004) Selective laser melting of iron-based powder. *J Mater Tech* 149:616–622. <https://doi.org/10.1016/j.jmatprotec.2003.11.051>
- Dev Singh D, Mahender T, Reddy AR (2021) Powder bed fusion process: a brief review. *Mater Today: Proc* 46:350–355. <https://doi.org/10.1016/j.matpr.2020.08.415>
- Thomas A, Fribourg G, Blandin JJ, Lhuissier P, Dendiev R, Martin G (2021) Effect of the build orientation on mechanical and electrical properties of pure Cu fabricated by E-PBF. *Addit Manuf* 48:102393. <https://doi.org/10.1016/j.addma.2021.102393>
- Blakey-Milner B, Gradl P, Snedden G, Brooks M, Pitot J, Lopez E, Leary M, Berto F, du Plessis A (2021) Metal additive manufacturing in aerospace: a review. *Mater Des* 209. <https://doi.org/10.1016/j.matdes.2021.110008>
- Emmelmann C, Kranz J, Herzog D, Wycisk E (2013) Laser additive manufacturing of metals. In: V. Schmidt, M.R. Beleggratis (Eds.), *Laser Technology in Bio-mimetics*, Springer, Heidelberg, 143–161. https://doi.org/10.1007/978-3-642-41341-4_6
- Davoodi E, Montazerian H, Mirhakimi AS, Zhianmanesh M, Ibhaddode O, Shahabad SI, Esmailizadeh R, Sarikhani E, Toorandaz S, Sarabi SA, Nasiri R, Zhu Y, Kakhodapour J, Li B, Khademhosseini A, Toyserkani E (2022) Additively manufactured metallic biomaterials. *Bioact Mater* 15:214–219. <https://doi.org/10.1016/j.bioactmat.2021.12.027>
- Kok Y, Tan XP, Wang P, Nai MLS, Loh NH, Liu E, Tor SB (2018) Anisotropy and heterogeneity of microstructure and mechanical properties in metal additive manufacturing: a critical review. *Mater Des* 139:565–586. <https://doi.org/10.1016/j.matdes.2017.11.021>
- Cooke S, Ahmadi K, Willerth S, Herring R (2020) Metal additive manufacturing: technology, metallurgy and modelling. *J Manuf Process* 57:978–1003. <https://doi.org/10.1016/j.jmapro.2020.07.025>
- Tran TQ, Chinnappan A, Lee JKY, Loc NH, Tran LT, Wang G, Kumar VV, Jayathilaka WADM, Ji D, Doddamani M, Ramakrishna S (2019) 3D printing of highly pure copper. *Metals* 9:756. <https://doi.org/10.3390/met9070756>
- Maleki E, Bagherifard S, Bandini M, Guagliano M (2021) Surface post-treatments for metal additive manufacturing: progress, challenges, and opportunities. *Addit Manuf* 37:101619. <https://doi.org/10.1016/j.addma.2020.101619>
- Jiang J, Chen J, Ren Z, Mao Z, Ma X, Zhang DZ (2020) The influence of process parameters and scanning strategy on lower surface quality of TA15 parts fabricated by selective laser melting. *Metals* 10:1228. <https://doi.org/10.3390/met10091228>
- Ikeshoji TT, Nakamura K, Yonehara M, Imai K, Kyogoku H (2018) Selective laser melting of pure copper. *JOM* 70:396–400. <https://doi.org/10.1007/s11837-017-2695-x>
- Gargalis L, Ye J, Strantz M, Rubenchik A, Murray JW, Clare AT, Ashcroft IA, Hague R, Matthews MJ (2021) Determining processing behaviour of pure Cu in Laser Powder Bed Fusion using direct micro-calorimetry. *J Mater Process Technol* 294:117130. <https://doi.org/10.1016/j.jmatprotec.2021.117130>
- Jiang D, Tian Y, Zhu Y, Huang A (2022) Investigation of surface roughness post-processing of additively manufactured nickel-based superalloy Hastelloy X using electropolishing. *Surf Coat Technol* 441:128529. <https://doi.org/10.1016/j.surfcoat.2022.128529>
- Bagehorn S, Wehr J, Maier HJ (2017) Application of mechanical surface finishing processes for roughness reduction and fatigue improvement of additively manufactured Ti-6Al-4V parts. *Int J Fatigue* 102:135–142. <https://doi.org/10.1016/j.ijfatigue.2017.05.008>
- Boschetto A, Bottini L, Macera L, Veniali F (2020) Post-processing of complex SLM parts by barrel finishing. *Appl Sci* 10:1382. <https://doi.org/10.3390/app10041382>
- Chyhyrynets E et al (2019) Vibro-tumbling as an alternative to standard mechanical polishing techniques for SRF cavities. *JaCoW Publishing* 464–466. <https://doi.org/10.18429/JACoW-SRF2019-TUP026>
- Bonesso M, Rebesan P, Gennari C, Mancin S, Dima R, Pepato A, Calliari I (2021) Effect of particle size distribution on Laser Powder Bed Fusion manufacturability of copper. *BHM Berg-und Hüttenmännische Monatshefte* 166:256–262. <https://doi.org/10.1007/s00501-021-01107-0>
- Benvenuti C, Calatroni S, Campisi IE, Darriulat P, Peck MA, Russo R, Valente AM (1999) Study of the surface resistance of superconducting niobium films at 1.5 GHz. *Phys C* 316:153–188. [https://doi.org/10.1016/S0921-4534\(99\)00207-5](https://doi.org/10.1016/S0921-4534(99)00207-5)
- Pira C et al (2019) Impact of the Cu substrate surface preparation on the morphological, superconductive and RF properties of the Nb superconductive coatings. *JaCoW Publishing* 935–940. <https://doi.org/10.18429/JACoW-SRF2019-THP041>
- Lanza G, Calatroni S, Marques Antunes Ferreira L, Gustafsson A, Pasini M, Trilhe P, Palmieri V (2009) The HIE-ISOLDE

- superconducting cavities: surface treatment and niobium film coating. Proceedings of SRF2009, Berlin, Germany. <https://accelconf.web.cern.ch/srf2009/papers/thppo075.pdf>.
22. Yang F, Zhang P, Dai J, Li Z (2020) OFHC copper substrate for niobium sputtering: comparison of chemical etching recipes. *Radiat Detect Technol Methods* 4:139–146. <https://doi.org/10.1007/s41605-020-00163-3>
 23. Tyagi P, Goulet T, Riso C, Stephenson R, Chuenprateep N, Schlitzer J, Benton C, Garcia-Moreno F (2019) Reducing the roughness of internal surface of an additive manufacturing produced 316 steel component by chemopolishing and electropolishing. *Addit Manuf* 25:32–38. <https://doi.org/10.1016/j.addma.2018.11.001>
 24. Shrivastava A, Kumar SA, Nagesha BK, Suresh TN (2021) Electropolishing of Inconel 718 manufactured by Laser Powder Bed Fusion: effect of heat treatment on hardness, ED surface topography and material ratio curve. *Opt Laser Technol* 144:107448. <https://doi.org/10.1016/j.optlastec.2021.107448>
 25. Maciąg T, Wiczorek J, Węcki B (2017) Parameters selection for electropolishing process of products made of copper and its alloys. *Arch Metall Mater* 62(3):1443–1447. <https://doi.org/10.1515/amm-2017-0223>
 26. Cooper C, Saito K, Bullock B, Joshi S, Palczewski A (2011) Centrifugal barrel polishing of cavities worldwide. Proceedings of SRF2011, Chicago, IL USA. <https://epaper.kek.jp/SRF2011/papers/weioa02.pdf>
 27. Gadelmawla ES, Koura MM, Maksoud TMA, Elewa IM, Soliman HH (2002) Roughness parameters. *J Mater Process Technol* 123:133–145. [https://doi.org/10.1016/S0924-0136\(02\)00060-2](https://doi.org/10.1016/S0924-0136(02)00060-2)
 28. Standard, British BS EN ISO 4287:1998 + A1:2009. Geometrical product specification (GPS) — surface texture: profile method — terms, definitions, and surface texture parameters. 2009.
 29. Yang F, Zhang P, Dai J, Li Z (2021) Surface preparation by mechanical polishing of the 1.3-GHz mono-cell copper cavity substrate prior chemical etching for niobium coating. *Radiat Detect Technol Methods* 5:33–41. <https://doi.org/10.1007/s41605-020-00215-8>

Publisher's note Springer Nature remains neutral with regard to jurisdictional claims in published maps and institutional affiliations.